Simulation of degraded wheel/rail adhesion conditions on a railway roller rig for the evaluation of the effect of wheel/roller contact on control performance

Monica Malvezzi, Enrico Meli, Luca Pugi

April 30, 2010

Abstract

In railway applications, the increasing speed, capacity and safety levels is leading to the introduction of complex mechatronic systems that monitor and control several aspects of train running. These complex subsystems have to be properly tested and in particular their interactions have to be carefully evaluated, expecially in particularly critical situations. The use of Hardware in The Loop techniques to simulate degraded adhesion conditions is a very fashionable matter, since this kind of tests are quite expensive and not very repeatable on real railway lines, in which the adhesion has to be degraded using water based contaminants solutions that have to be applied and then removed from the line once the test has been concluded. The physical reproduction of degraded adhesion conditions on roller rigs using contaminants is not practically feasible, since if heavy sliding occurred rolling surface of the rollers could be damaged

or worn causing an unacceptable increase of costs and a reduced availability of the plant. Furthermore both on track and on roller test rig the simulations of long slidings conditions with prolonged and deterministic testing conditions is quite impossible.

The authors in some previous works described the features of a locomotive full scale roller rig for the simulation of degraded adhesion conditions between the wheel and the simulated rail, the design of the rig control system was based on the hypotheses that the contact between the roller and the wheel may be considered as a pure rotating constraint, while the loss of adhesion is simulated by modulating the torque applied to the roller motor in order to reproduce the same speed profiles that the wheel would have in the reality. The importance of the proposed applications and the difficulty to simulate complex interactions between many mechatronic subsystems, sensors and actuators justified further effort in the design of a scaled version of the rig that will be used to speed up the prototyping of the control algorithms and models that will be used on the full scale test rig currently in the realization phase.

The control law performance of both the full scale and the scaled roller rig is substantially based on the hypothesis that no sliding occur between the wheel and the roller, but the pure rotating constraint between the wheel and the roller is only approximately guaranteed and highly depends on the force distribution in the wheel/roller contact area: a sliding between the rolling surfaces may arise if the applied torque increases or in presence of dynamic effect (high accelerations), that could be present when degraded adhesion conditions are simulated, due to the intervention of anti-slip and wheel slide protection system. Furthermore the rig control system may be affected by the dynamic of the roller in the lateral direction. So further analysis were performed in order to understand if the previously neglected phenomena can play a significant role on the roller rig control system. This is the motivation of the development of a detailed multibody model of the scaled roller rig and scaled bogie. The numerical model includes the three dimensional dynamics of the system, the actuator transfer functions and the roller and bogie motor control systems. A particular attention was devoted to the model of the wheel/roller contact, since we need to evaluate the effect of local sliding and of the position of the wheel/rail contact point on the dynamics of the whole system. For this purpose the wheel/rail contact model described in has been adapted to a scaled wheel/roller contact.

The paper will present the features of the scaled roller rig and will explain the main details of the developed simulation model, with a particular attention to the wheel/roller contact model, then the results of some numerical tests will be presented, the test results will be used to discuss the effectiveness of the proposed control laws.

Keywords: roller rig, degraded adhesion, multibody simulation.

1 Introduction

In railway applications, the testing of on-board components is necessary to optimize the efficiency of the systems and to allow high safety levels. The introduction of mechatronic device to control and manage different running conditions is nowadays common in the railway practice. The analysis of the possible interactions between all these subsystems has to be carefully investigated by simulations and experimental tests. In order to reduce the time and the cost of the testing phase, the use of dedicated test rigs is often encouraged. Test rigs dedicated to specific on board devices are rather frequent in the railway practice, for example for ATP/ATC on board or WSP system [2],[3],[9]. Beside the single component, also the mutual interaction between subsystems has to be evaluated. In order to perform this type of validation locomotive roller rigs can be used. Some studies for the realization of a full-scale locomotive roller rig devoted to the simulation of degraded adhesion conditions between the wheel and the rail has been recently presented [5]. The main mechanical and control problems that arise in the design of this type of test rig have been highlighted, and in particular, the feasibility of tests with degraded adhesion conditions between the wheel and the rail is simulated.

Tests in which degraded adhesion conditions are simulated are quite expensive and not very repeatable on real railway lines in which the adhesion has to be degraded using water based contaminants solutions that have to be applied and then removed from the line once the test has been concluded. The physical reproduction of degraded adhesion conditions on roller rigs using contaminants is not practically feasible, since if heavy sliding occurred rolling surface of the rollers could be damaged or worn causing an unacceptable increase of costs and a reduced availability of the plant. Furthermore both on track and on roller test rig the simulations of long slidings conditions with prolonged and deterministic testing conditions is quite impossible. The authors in some previous works [5] described the features of a full scale roller rig for the simulation of degraded adhesion conditions between the wheel and the simulated rail, the design of the rig control system was based on the hypotheses that the contact between the roller and the wheel may be considered as a pure rotating constraint, while the loss of adhesion is simulated by modulating the torque applied to the roller motor in order to reproduce the same speed profiles that the wheel would have in the reality. Some simulations of the proposed systems have been previously performed on models developed, however the importance of the proposed applications and the difficulty to simulate complex interactions between many mechatronic subsystems, sensors and actuators justified further effort in the design of a scaled version of the rig that will be used to speed up the prototyping of the control algorithms and models that will be used on the full scale test rig currently in the realization phase. The scaled bogie is sketched in figure 1, since the dimension of the scaled bogie are limited, the installation of both the traction and the braking system was not practically feasible, so the two bogie motors simulate both the traction and the braking force, as shown in the Figure 2 block diagram.

In the design phase of the test rig an analysis of the roller rig dynamics is funda-

mental to verify the feasibility of degraded adhesion tests, to investigate the behavior of the scaled bogie on the rig, to test and validate different control strategies. For these reasons in the design phase of the scaled roller rig a multibody model of the system has been realized. The key points of this model are the interaction with the control system and the wheel/roller contact model.

The paper presents the numerical model of the system dynamics, including the multibody system dynamics, control system and electromechanical component dynamics. The model has been developed in the Matlab-Simulink environment. some numerical simulations will be presented in order to show the behavior of the scaled bogie on the rig when low adhesion conditions are simulated.

The control law performance of both the full scale and the scaled roller rig described in [5] is substantially based on the hypothesis that no sliding occur between the wheel and the roller. On the other hand the pure rotating constraint between the wheel and the roller is only approximately guaranteed and highly depends on the force distribution in the wheel/roller contact area: a sliding between the rolling surfaces may arise if the applied torque increases or in presence of dynamic effect (high accelerations), that could be present when degraded adhesion conditions are simulated, due to the intervention of anti-slip and wheel slide protection system. Furthermore the rig control system may be affected by the dynamic of the roller in the lateral direction. So further analysis are necessary in order to understand if the phenomena previously neglected can play a significant role on the roller rig control system. This is the motivation of the development of a detailed multibody model of the scaled roller rig and scaled bogie. The numerical model includes the three dimensional dynamics of the system, the actuator transfer functions and the roller and bogie motor control systems.

A particular attention was devoted to the model of the wheel/roller contact, since we need to evaluate the effect of local sliding and of the position of the wheel/rail contact point on the dynamics of the whole system. For this purpose the wheel/rail contact model described in [8],[1] has been adapted to a wheel/roller contact. This contact model has been developed in the Matlab/Simulink environment and thus is particularly suitable to be integrated within a model in which the system dynamics is strictly connected to the behavior of electromechanic elements and control logics. In the contact model the location of contact points is defined by semi-analytic algorithms that find the minimum distance between the contact surfaces: on the basis of the relative indentation between the contact surfaces the normal load distribution is evaluated, while on the basis of the relative speed between the contact surface in the contact point the tangential component of the contact force is evaluate.

The paper will present the details of the developed simulation model, with a particular attention to the wheel/roller contact model, then the results of some numerical tests will be presented, the test results will be used to discuss the effectiveness of the proposed control laws.

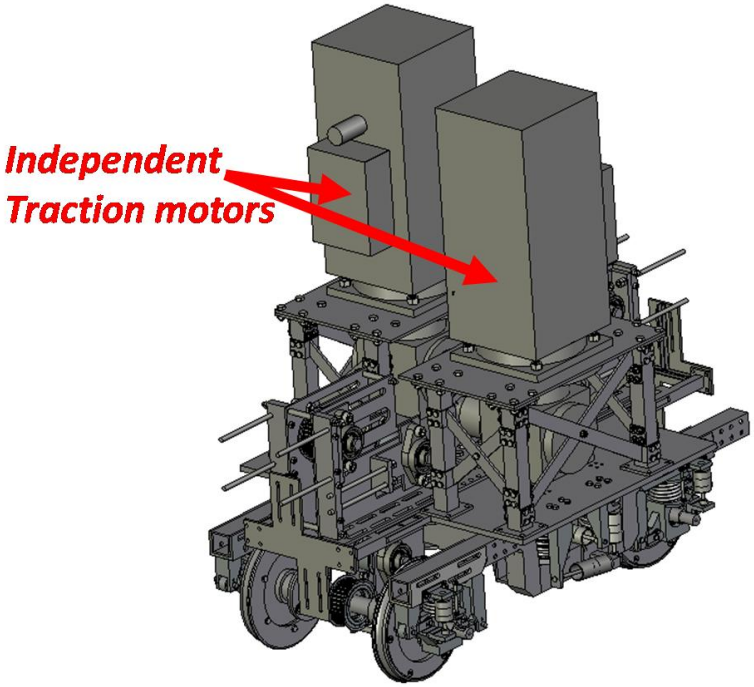

Figure 1: The scaled bogie: layout of the mechanical design.

2 The multibody model

In this study we analysed and compared the performance of a bogie on a full scale test rig with those that the same bogie would have on a real track. We considered as benchmark vehicle the MMU [4]. This vehicle has been chosen because several simulations and tests were performed with, so the available model was validated. Furthermore we chosen the full scale case because in future devlopments we intend to improve the roller rig control simulator described in [5] with a complete three dimensional multibody model of the tested vehicle and to consider the complete three dimensional geometry in the contact between the rollers and the wheels.

The multibody model of the bogie on the roller rig is composed of five rigid bodies: the bogie, two wheelsets and two rollers; the wheelset are connected to the bogie by three-dimensional non linear elastic-viscous force elements modeling the primary suspensions, while the bogie is connected to a fixed body (representing the car body, whose motion is not considered in this set of preliminary test), by three-dimensional non linear elastic-viscous force elements reproducing the primary suspensions.

The numerical procedure was realized in the MATLAB-Simulink environment, that is particularly suitable in this case, since the multibody model will be used in future applications to test and compare control algorithms both for the full scale and for the scaled roller rig. The chosen environment allows to obtain a numerically efficient model, to test different types of integration algorithms, and to manage singularities.

The structure of the numerical tool is modular and parametric so different subsystems can be easily modeled and substituted in the main procedure. In this type of design environment, different and complex systems can be modeled (electrical, pneumatic etc.), while a toolbox devoted to the multibody simulation allows to easily model mechanical systems with an high number of bodies and constraints. The model can be easily customized and personalized in order to introduce several railway mechatronic subsystems, as for example anti-skid and anti-slip devices, braking and traction systems.

The wheel-roller interaction model considers a full three dimensional rolling contact and can manage multiple contact points. On each wheelset the following forces and torques act:

- the creep forces in the contact area (T_x^b,T_y^b);
- the forces due to the interaction with the boogie (S_r^b, S_l^b);
- the external applied braking or traction torque C^b;
- the weight.

Consequently on each roller the following forces and torques will act:

- the creep forces in the contact area ($-T_x^b$,$-T_y^b$);
- the forces due to the interaction with the roller supports;
- the roller applied braking or traction torque C;
- the roller weight.

3 The Contact Model

One of the key point of this simulation is the model of the wheel/roller contact. The implemented model was substantially adapted from those presented in previous works [8],[7],[6], due to its reliability and computational performance. The method was based on the analythical research of the stationary points of a function describing the distance between the contact surfaces. A *fixed reference* system $O_b x_b y_b z_b$ is defined, its origin is on the roller rotation axis, on the roller profile symmetry plane, and the axis y_b is parallel to the rotation axis. The *local reference system* $O_r x_r y_r z_r$ is defined on the wheelset. The y_r axis is coincident with the rotation axis of the wheels and is rigidly connected to the axle (except for the rotation around this axis). The x_r axis is contained in the plane $x_b y_b$ and the origin O_r coincides with the center of mass G of the wheelset. The position and orientation of the local reference system with respect to the fixed one can be described by the vector $\mathbf{o}_r^b$, that includes the O_r coordinates with respect to $O_b x_b y_b z_b$ and the rotation matrix $[\mathbf{R}]$.

In the local system the axle (and therefore the wheels) can be described by means of a revolution surface. The generative function, schematically sketched in Figure 4 a), is indicated with $r(y_r)$ (the function $r(y_r)$ is known).

The position of a generic point of the wheel profile in the local reference frame has consequently the following analytic expression:

$$\mathbf{p}_r^r(x_r, y_r) = \begin{pmatrix} x_r \\ y_r \\ -\sqrt{r(y_r)^2 - x_r^2} \end{pmatrix}. \tag{1}$$

while the position of the same point in the roller reference system is given by:

$$\mathbf{p}_r^b(x_r, y_r) = \mathbf{o}_r^b + \mathbf{R}\mathbf{p}_r^r(x_r, y_r) \tag{2}$$

Similarly the roller can be described in the fixed reference system by means of a revolution surface. The generative function, indicated with $b(y_b)$ is known and is sketched in Figure 4 b).

The position of a generic point of the rail surface in the auxiliary system are:

$$\mathbf{p}_b^b(x_b, y_b) = \begin{pmatrix} x_b \\ y_b \\ \sqrt{b(y_b)^2 - x_b^2} \end{pmatrix}. \tag{3}$$

For both surfaces the normal unitary vectors (outgoing for convention) can be defined. The normal unitary vector on the wheel surface (Figure 5 a)) is defined, in the local system, as follows:

$$\mathbf{n}_r^r(\mathbf{p}_r^r) = -\left(\frac{\partial \mathbf{p}_r^r}{\partial x_r} \wedge \frac{\partial \mathbf{p}_r^r}{\partial y_r}\right) / \left\| \frac{\partial \mathbf{p}_r^r}{\partial x_r} \wedge \frac{\partial \mathbf{p}_r^r}{\partial y_r} \right\| \tag{4}$$

whereas, in the fixed reference system, the unitary vector is defined as:

$$\mathbf{n}_r^b(\mathbf{p}_r^b) = \mathbf{R}\mathbf{n}_r^r(\mathbf{p}_r^r). \tag{5}$$

The unitary vector relative to the roller surface (Figure 5 b)), with respect to the auxiliary system is defined as:

$$\mathbf{n}_b^b(\mathbf{p}_b^b) = \left(\frac{\partial \mathbf{p}_b^b}{\partial x_b} \wedge \frac{\partial \mathbf{p}_b^b}{\partial y_b}\right) / \left\| \frac{\partial \mathbf{p}_b^b}{\partial x_b} \wedge \frac{\partial \mathbf{p}_b^b}{\partial y_b} \right\| \tag{6}$$

The method used to locate the contact points between the roller and the wheel is based on the idea that the in each contact point the distance between the wheel surface and the rail surface assumes a local maximum. The problem can be efficiently solved imposing the following conditions (Figure 6)[**?**]:

- the normal unitary vector relative to the roller surface $\mathbf{n}_b^b(\mathbf{p}_b^b)$ has to be parallel to the wheel surface normal unitary vector $\mathbf{n}_r^b(\mathbf{p}_r^b)$:

$$\mathbf{n}_b^b(\mathbf{p}_b^b) \times [\mathbf{R}]\mathbf{n}_r^r(\mathbf{p}_r^r) = \mathbf{0} \quad ; \tag{7}$$

- the roller surface normal unitary vector $\mathbf{n}_b^b(\mathbf{p}_b^b)$ has to be parallel to the vector $\mathbf{d}^b$ representing the distance between the generic point of the wheel and of the rail :

$$\mathbf{n}_b^b(\mathbf{p}_b^b) \times \mathbf{d}^b = \mathbf{0} \quad . \tag{8}$$

The vector $\mathbf{d}^b$ can be expressed as:

$$\mathbf{d}^b(x_r, y_r, x_b, y_b) = \mathbf{p}_r^b(x_r, y_r) - \mathbf{p}_b^b(x_b, y_b) = \mathbf{o}_r^b + [\mathbf{R}]\mathbf{p}_r^r(x_r, y_r) - \mathbf{p}_b^b(x_b, y_b). \tag{9}$$

$\mathbf{d}^r(x_r, y_r, x_b, y_b)$ depends on four parameters, namely the parameters used to identify a point on the rail and on the wheel surface respectively. The conditions defined in (7) and (8) represent a system composed of six equations (since two vectorial constraints are imposed) and four unknowns (x_r,y_r,x_b,y_b), then only four of them are independent. The parallelism constraints expressed in the equations (7) and (8) by means of a cross product could be described imposing the orthogonality between the unitary vectors $[\mathbf{R}]\mathbf{n}_r^r(\mathbf{p}_r^r)$ and $\mathbf{d}^b(x_r, y_r, x_b, y_b)$ and the plane tangent to the rail in $\mathbf{p}_b^b$. Each of these conditions can be expressed by means of two dot products, then the over mentioned conditions can be represented by four scalar equations. We adopted the previously described formulation because it leaded to a simpler form of the analytical expressions.

The four dimensional system has been analytically reduced to a single unknown equation, that has then be solved numerically.

The solutions of the system (7-8) are indicated with

$$(x_{ri}^C, y_{ri}^C, x_{bi}^C, y_{bi}^C), \quad i = 1, 2, ...n \quad , \tag{10}$$

and the corresponding contact points on the wheel and on the rail (Figure **??**) are;

$$\mathbf{p}_{ri}^{b,C} = \mathbf{p}_r^b(x_{ri}^C, y_{ri}^C), \quad \mathbf{p}_{bi}^{b,C} = \mathbf{p}_b^b(x_{bi}^C, y_{bi}^C), \quad i = 1, 2, ...n \quad . \tag{11}$$

Some further controls allow to verify that the solutions are physically realistic, in the analytic development no simplifications and approximations were assumed then no solution of the problem should be excluded:

1. research and elimination of the multiple solutions;
2. check of the analytic conditions (the solutions have to be real);
3. check of the condition on the curvatures;

4. check of the condition on the normal indentation.

For each contact point $\mathbf{p}_b^{b,C}$ (the index i has been omitted for brevity) the contact forces can be calculated, in particular:

1. the normal component of the contact force, as a function of the relative indentation between the contact surfaces in the contact area: $\mathbf{N}^b(\mathbf{p}_b^{b,C}) = N^b(\mathbf{p}_b^{b,C})\mathbf{n}_b^b(\mathbf{p}_b^{b,C})$;
2. the tangential contact forces, that depends on the normal component and on the relative kinematics between the wheel and the roller: $\mathbf{T}_x^b(\mathbf{p}_b^{b,C}) = T_x^b(\mathbf{p}_b^{b,C})\mathbf{i}_b$ and $\mathbf{T}_y^b(\mathbf{p}_b^{b,C}) = T_y^b(\mathbf{p}_b^{b,C})\mathbf{t}_b^b(\mathbf{p}_b^{b,C})$ where $\mathbf{t}_b^b(\mathbf{p}_b^{b,C}) = \mathbf{n}_b^b(\mathbf{p}_b^{b,C}) \wedge \mathbf{i}_b$;
3. the spin moment $\mathbf{M}_{sp}^b(\mathbf{p}_b^{b,C}) = M_{sp}^b(\mathbf{p}_b^{b,C})\mathbf{n}_b^b(\mathbf{p}_b^{b,C})$.

Both the contact forces and the spin moment are conventionally exercised by the roller on the wheel and are expressed in the roller reference system. As regards the normal contact force, according to the Hertz theory, the relation 12 holds

$$N^b(\mathbf{p}_b^{b,C}) = \left[-k_h \left|\tilde{p}_n\right|^\gamma + k_v \left|v_n\right| \frac{sign(v_n) - 1}{2}\right] \frac{sign(\tilde{p}_n) - 1}{2} \tag{12}$$

where $\gamma = 3/2$, $k_v = 10^5 Ns/m$, $v_n = \mathbf{v} \bullet \mathbf{n}_b^b(\mathbf{p}_b^{b,C})$ and $\mathbf{v} = \dot{\mathbf{G}}^b + \omega^b \wedge (\mathbf{p}_b^{b,C} - \mathbf{G}^b)$. The hertzian constant k_h can be evaluated as follows

$$k_h = \frac{2\pi}{3Q} \frac{1}{\sqrt{D_1 + D_2}} \frac{\sqrt{E(g)}}{gK(g)^{3/2}} \tag{13}$$

with $Q = \frac{1-v}{G}$ (here G is the tangential modulus of elasticity and ν the Poisson coefficient; the used values are $G = 10^{10} Pa$ and $\nu = 0.3$ both for the wheel and the rail). The parameters D_1 and D_2 are defined as

$$D_1 = \tfrac{1}{2}(k_{1r}(y_r^C) + k_{1b}(y_r^b(x_r^C, y_r^C))) \quad D_2 = \tfrac{1}{2}(k_{2r}(y_r^C) + k_{2b}(y_r^b(x_r^C, y_r^C))) \tag{14}$$

where k_{1r} and k_{2r} are the normal curvatures of the wheel surface in longitudinal and lateral direction while k_{1b} and k_{2b} are the analogous curvatures of the roller surface. As is usual in the rolling contact, the principal directions of curvatures of the two surfaces are almost coinciding in the contact point; consequently the normal curvatures assume the form:

$$\begin{aligned}
&k_{1r}(y_r^C) \simeq K_{1r}(y_r^C) = \tfrac{1}{|r(y_r^C)|\sqrt{1+r'(y_r^C)^2}}, \\
&k_{1b}(y_r^b(x_r^C, y_r^C)) \simeq K_{1b}(y_r^b(x_r^C, y_r^C)) = 0, \\
&k_{2r}(y_r^C) \simeq K_{2r}(y_r^C) = \tfrac{r''(y_r^C)}{(1+r'(y_r^C)^2)^{3/2}}, \\
&k_{2b}(y_r^b(x_r^C, y_r^C)) \simeq K_{2b}(y_r^b(x_r^C, y_r^C)) = \tfrac{-b''(y_r^b(x_r^C, y_r^C))}{\left(1+b'(y_r^b(x_r^C, y_r^C))^2\right)^{3/2}}.
\end{aligned} \tag{15}$$

where this time K_{1r}, K_{2r}, K_{1b} and K_{2b} are the principal normal curvatures of the wheel and of the rail.

The axial ratio g of the contact ellipse is defined as $g = \min\left(\frac{a}{b}, \frac{b}{a}\right)$ (where a and b are the longitudinal and the lateral semi-axes) and can be found solving the equation

$$\frac{|D_1 - D_2|}{D_1 + D_2} = \left(1 - g^2\right) \frac{D(g) - C(g)}{E(g)}. \tag{16}$$

If $a_m = \min(a, b)$ and $a_M = \max(a, b)$ are the minor and the major of the contact ellipse semi-axes, the relations (17) hold

$$a_m = \sqrt{\frac{\tilde{p}_n}{D_1 + D_2} \frac{E(g)}{K(g)}}, \quad a_M = \frac{a_m}{g}. \tag{17}$$

The comparison between the parameters D_1 and D_2 allows to determine the exact values of the semi-axes a and b:

$$D_1 \leq D_2 \Rightarrow \begin{cases} a = a_M \\ b = a_m \end{cases} \quad D_1 \geq D_2 \Rightarrow \begin{cases} a = a_m \\ b = a_M \end{cases} \tag{18}$$

The functions $C(g)$, $D(g)$, $E(g)$ and $K(g)$ introduced above are the following elliptic integrals

$$\begin{aligned} C(g) &= \int_0^{\pi/2} \sin(t)^2 \cos(t)^2 \left(1 - (1 - g^2)\sin(t)^2\right)^{-3/2} dt \\ E(g) &= \int_0^{\pi/2} \left(1 - (1 - g^2)\sin(t)^2\right)^{1/2} dt \\ D(g) &= \int_0^{\pi/2} \sin(t)^2 \left(1 - (1 - g^2)\sin(t)^2\right)^{-1/2} dt \\ K(g) &= \int_0^{\pi/2} \left(1 - (1 - g^2)\sin(t)^2\right)^{-1/2} dt \end{aligned} \tag{19}$$

that can be found tabulated in literature. The tangential contact forces and the spin moment can be instead calculated by means of the Kalker linear theory:

$$\begin{aligned} \widetilde{T}_x^b(\mathbf{p}_b^{b,C}) &= -f_{11}\epsilon_x \\ \widetilde{T}_y^b(\mathbf{p}_b^{b,C}) &= -f_{22}\epsilon_y - f_{23}\epsilon_{sp} \\ M_{sp}^b(\mathbf{p}_b^{b,C}) &= f_{23}\epsilon_y - f_{33}\epsilon_{sp} \end{aligned} \tag{20}$$

where ϵ_x, ϵ_y and ϵ_{sp} are the longitudinal, the lateral and the spin creepages defined as

$$\varepsilon_x = \mathbf{v} \bullet \mathbf{i}_b \Big/ || \dot{\mathbf{G}}^b ||, \quad \varepsilon_y = \mathbf{v} \bullet \mathbf{t}_b^b(\mathbf{p}_b^{b,C}) \Big/ || \dot{\mathbf{G}}^b ||, \quad \varepsilon_{sp} = \omega^b \bullet \mathbf{n}_b^b(\mathbf{p}_b^{b,C}) \Big/ || \dot{\mathbf{G}}^b ||. \tag{21}$$

The coefficients f_{ij} can be expressed as a function of the materials and of the contact ellipse semi-axes

$$\begin{aligned} f_{11} &= abGC_{11} \qquad f_{22} = abGC_{22} \\ f_{23} &= (ab)^{3/2} GC_{23} \quad f_{33} = (ab)^2 GC_{33} \end{aligned} \tag{22}$$

while the values of the Kalker's constants $C_{ij}(\nu, g)$ are available in literature. Finally, since the Kalker linear theory does not consider the adhesion limit, a saturation on the magnitude of the tangential contact force $\widetilde{T}^b = \sqrt{\widetilde{T}_x^{b\,2} + \widetilde{T}_y^{b\,2}}$ has to be introduced. In other words $\widetilde{T}^b$ can not exceed the pure slip value $T_s^b = \mu N^b$ where μ is the kinematic friction coefficient. For this purpose the saturation coefficient ε is defined:

$$\varepsilon = \begin{cases} \frac{T_s^b}{\widetilde{T}^b} \left[\left(\frac{\widetilde{T}^b}{T_s^b} \right) - \frac{1}{3} \left(\frac{\widetilde{T}^b}{T_s^b} \right)^2 + \frac{1}{27} \left(\frac{\widetilde{T}^b}{T_s^b} \right)^3 \right] & \widetilde{T}^b \leq 3T_s^b \\ \frac{T_s^b}{\widetilde{T}^b} & \widetilde{T}^b > 3T_s^b. \end{cases} \tag{23}$$

The saturated components of the tangential contact forces can be calculated as follows:

$$\begin{aligned} T_x^b &= \varepsilon \widetilde{T}_x^b \\ T_y^b &= \varepsilon \widetilde{T}_y^b. \end{aligned} \tag{24}$$

4 Preliminary numerical Simulation

A first set of numerical simulations, that are described in this paper, are devoted to validate the developed numerical model. First a series of simulations were performed to analyze on the roller rig the bogie critical speed. Figure 7 shows some of the obtained results: figure 7 a) shows the lateral displacement of the bogie as a function of the longitudinal (simulated) speed. As it can be seen, the behavior is stable for speeds lower than 100 km/h and instable for higher speed values. Figure 7 b) shows the frequency of the oscillations as a function of the longitudinal speed, for a full vehicle on the rails and for a bogie on the roller rig. The results shows that both the frequency of the oscillations and the critical speed obtained simulating the bogie on the rig are similar to those obtained with the full vehicle on the rails [6]. This set of tests were devoted to validate the multibody model and to compare the results obtained on the test rig wth those obtained on the line.

One of the main purposes of the developed multibody model was the validation of the control laws described in [5], that were obtained assuming a pure rolling constraint between the wheel and the roller and were tested on a simplified bidimensional multibody model. A second set of tests were performed in order to highlight the longitudinal sliding between the wheel and the roller, that may affect the roller control

performance. In this series of tests, starting from a reference speed, a traction torque was added to the bogie wheels. The applied torque is null in the first simulation second, then increases linearly up to a maximum value, reached after 5 seconds from the simulation starting instant, and then it's kept constant. Figure 8 shows some of the obtained results: figure 8 a) shows the front and rear right wheel absolute sliding during the simulation. Only the results relative to the right wheels have been plotted, since in this simulation the results where symmetrical for the left side wheels. The absolute sliding is initially null, when no torque is applied, then, while the torque is linearly increased, the sliding grows following a second order curve, then, in the final part of the simulation, when the applied torque is constant, it increases linearly. Figure 8 shows the longitudinal and vertical component of the contact force, for the front and read right wheel. The longitudinal components follow the behavior of the applied torque, while the vertical components, initially have the same value and then, due to the application of the external torque, assumes two linearly moves to the different values.

5 Conclusion and future developments

The paper describes the main features and the results of some preliminary tests of the multibody model of a railway bogie on a roller rig. The multibody simulation is necessary to investigate the dynamical behavior of the test rig, to analyze system stability and to test and develop suitable control strategies. A particular attention has been devoted to the model of the roller/wheel contact pair: a semi-analytic procedure developed for the wheel/rail pair has been adapted to the wheel/roller contact problem to find the contact points between the wheels and the rollers. The contact forces were then evaluated as a function of the normal indentation between the contact surfaces and of the relative kinematics between the roller and the wheel, according to Hertz and Kalker theories. The contact model has been integrated within the multibody model of the rig and some preliminary simulations have been performed. The research activity is still going on and future analysis will be performed in order to verify the effect of roller/wheel contact in the stability and performance of roller control systems previously defined, that were based on the hypothesis that a perfect rolling constraint between the rollers and the wheels, in particular when degraded adhesion conditions are simulated.

References

[1] AUCIELLO, J., MELI, E., FALOMI, S., AND MALVEZZI, M. Dynamic simulation of railway vehicles: wheel/rail contact analysis. *Vehicle System Dynamics 47*, 7 (July 2009), 867–899.

[2] F. SONG, A. FOLLECO, E. A. High fidelity hardware-in-the-loop simulation development for an autonomous underwater vehicle. In *OCEANS* (Vol. 1, pp. 444 -449, 2001), M. Conference and Exhibition, Eds.

[3] HANSELMANN, H. Hardware-in-the-loop simulation testing and its integration into a cacsd toolset,. In *Proceedings of the IEEE International Symposium on Computer-Aided Control System Design* (pp. 152 -156, 1996), I. Conference and Exhibition, Eds.

[4] IWNICKI, S. *The Manchester Benchmarks for Rail Vehicle Simulators*. Swets & Zeitlinger, Lisse, Netherlands, 1999.

[5] M., M., B., A., AND L., P. Feasibility of degraded adhesion tests in a locomotive roller rig. *Proceedings of the Institution of Mechanical Engineering, Part F 222* (2008), 27–43.

[6] MALVEZZI, M., MELI, E., AUCIELLO, J., AND FALOMI, S. Dynamic simulation of railway vehicles: wheel - rail contact analysis. *Vehicle System Dynamics 47*, 7 (2009), 867–899.

[7] MELI, E., FALOMI, S., MALVEZZI, M., AND RINDI, A. Determination of wheel - rail contact points with semianalytic methods. *Multibody System Dynamics 20*, 4 (2008), 327–358.

[8] MELI, E., MALVEZZI, M., PAPINI, S., PUGI, L., RINCHI, M., AND RINDI, A. A railway vehicle multibody model for real-time applications. *Vehicle System Dynamics 46*, 12 (Dec. 2008), 1083–1105.

[9] PUGI, L., MALVEZZI, M., TARASCONI, A., PALAZZOLO, A., AND VIOLANI, M. Hil simulation of wsp systems on mi-6 test rig.

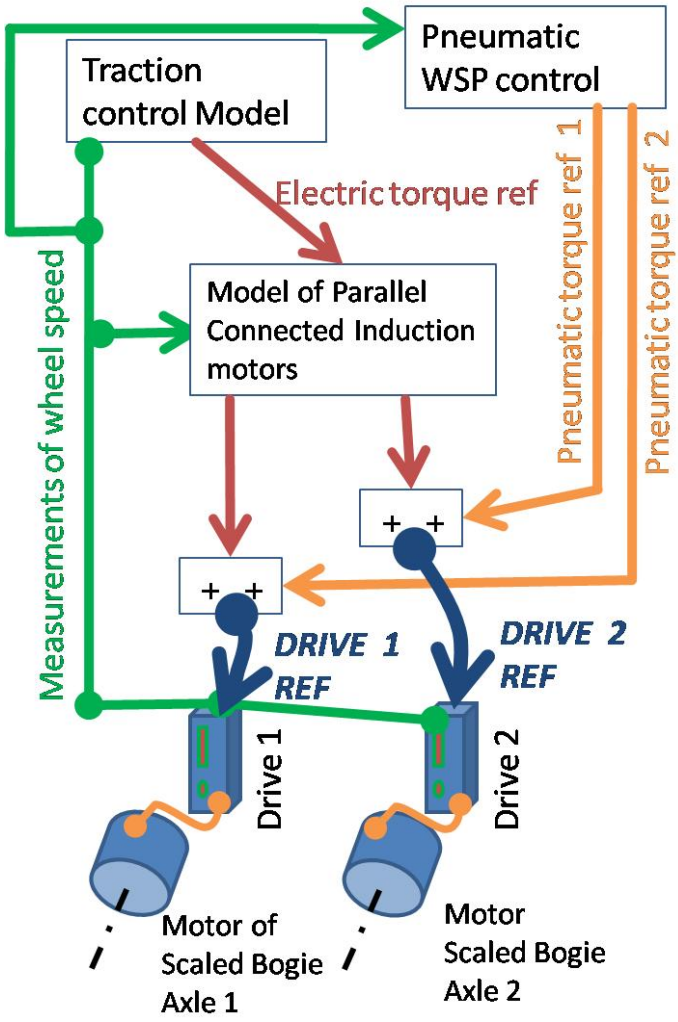

Figure 2: The scaled bogie: the scaled bogie motors working as brakes, the block diagram shows how the braking force is simulated controlling the torque of scaled bogie motors.

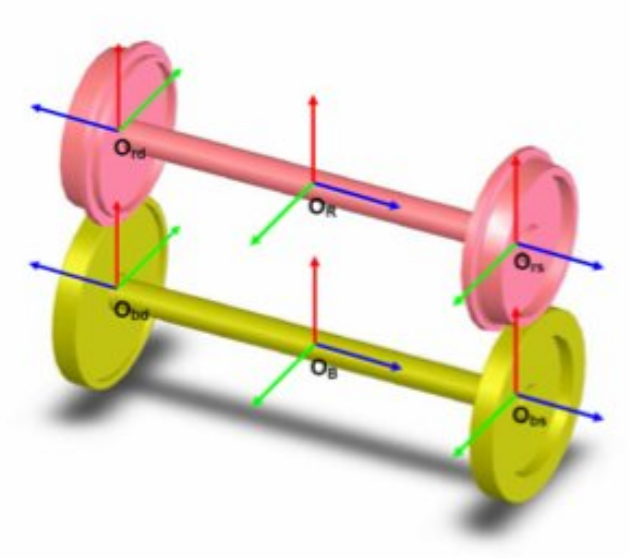

Figure 3: Overview of the multibody model: the wheelset and the roller.

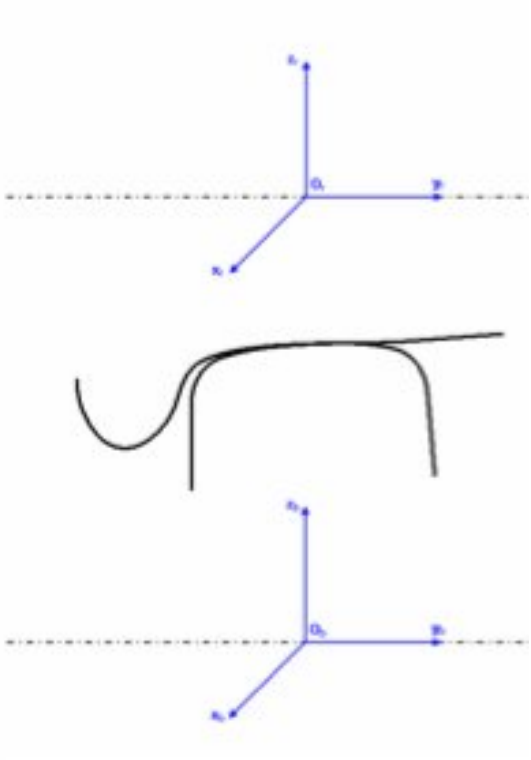

Figure 4: Generative function of the wheelset and the roller.

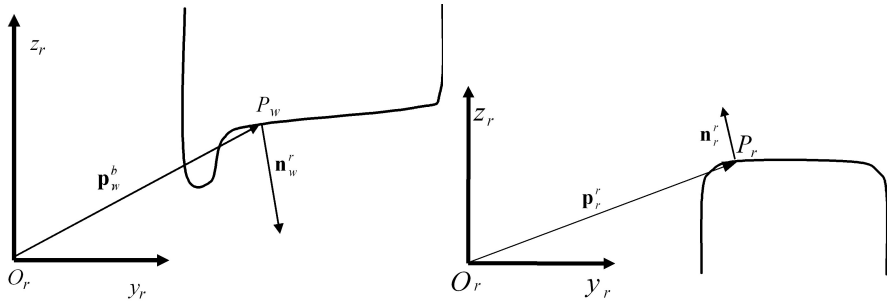

Figure 5: a) Normal unitary vector of the axle. b) Normal unitary vector of the roller.

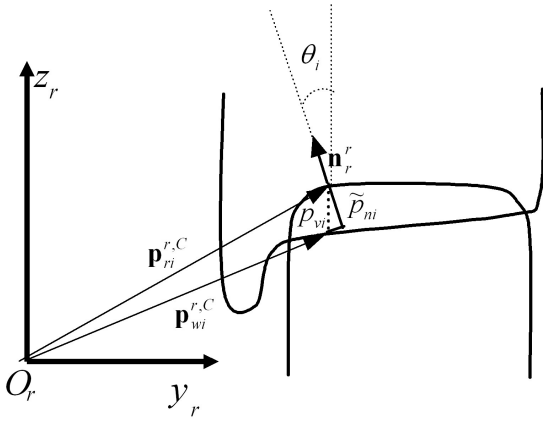

Figure 6: Identification of the contact points between the wheel and the roller.

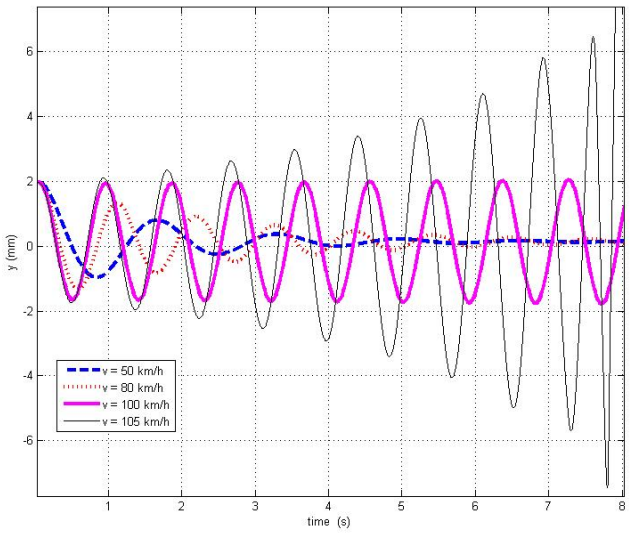

a)

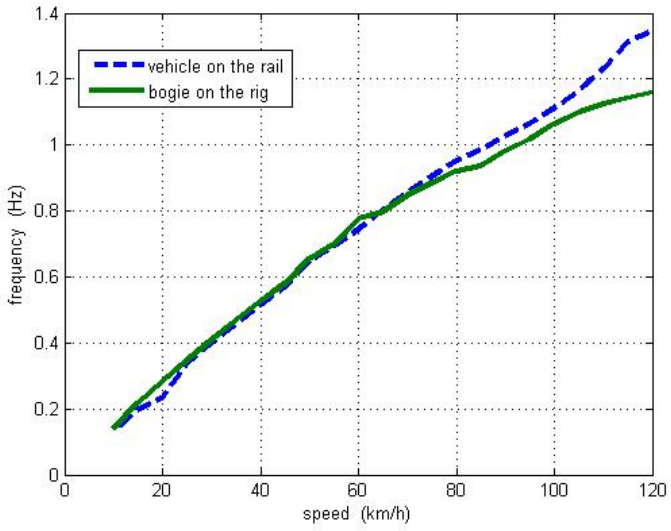

b)

Figure 7: a) Lateral displacement of the bogie on the rig as a function of the longitudinal (simulated) speed, as it can be seen, for speeds greater than 100 km/h the oscillation tends to amplify thus the system is unstable. b) Frequency of the lateral oscillation as a function of the longitudinal speed, comparison between the results obtained simulating a full vehicle on the rails and a single bogie on the rig.

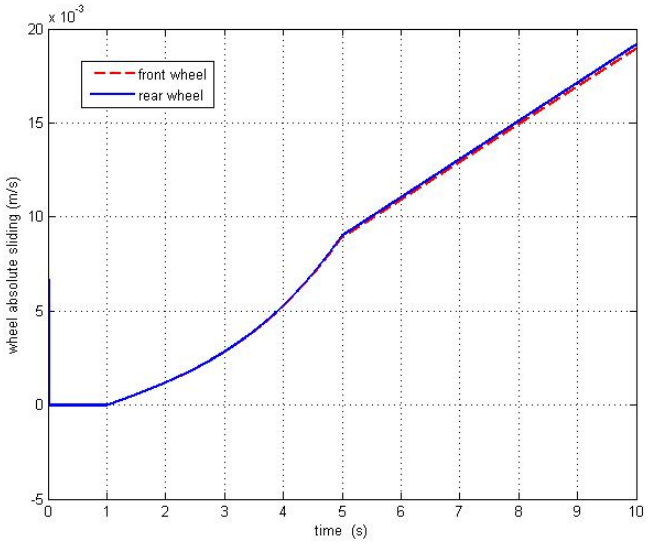

a)

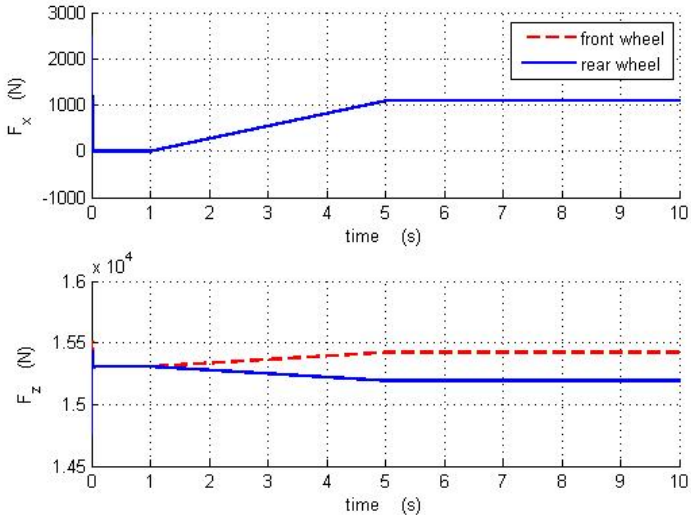

b)

Figure 8: a) absolute sliding in the front and rear right wheel during a traction test. b) longitudinal and vertical component of the contact force on the front and rear right wheel during the traction test.